European Journal of Immunology

Proteome analysis of human CD56^{neg} NK cells reveals a homogeneous phenotype surprisingly similar to CD56^{dim} NK cells

Jenny Voigt[1*], David F.G. Malone[2*], Joana Dias[2], Edwin Leeansyah[2,4], Niklas K. Björkström[2], Hans-Gustaf Ljunggren[2], Lothar Gröbe[1], Frank Klawonn[1,3], Maxi Heyner[1], Johan K. Sandberg[2#] and Lothar Jänsch[1#]

[1]Cellular Proteomics, Helmholtz Centre for Infection Research, Braunschweig, Germany

[2]Center for Infectious Medicine, Department of Medicine Huddinge, Karolinska Institutet, Karolinska University Hospital, Stockholm, Sweden

[3]Department of Computer Science, Ostfalia University of Applied Sciences, Wolfenbuettel, Germany

[4]Program in Emerging Infectious Diseases, Duke-National University of Singapore Medical School, Singapore

*Joint first authors

#Joint corresponding authors:

Lothar Jänsch, Inhoffenstraße 7, 38124 Braunschweig, Germany, phone: +49 6181 3030, e-mail: Lothar.Jaensch@helmholtz-hzi.de

Johan Sandberg, CIM, Department of Medicine, F59, Karolinska Institutet, Karolinska University Hospital Huddinge, 141 86 Stockholm, Sweden, e-mail: Johan.Sandberg@ki.se

Received: 11/12/2017; Revised: 07/05/2018; Accepted: 04/07/2018
This article has been accepted for publication and undergone full peer review but has not been through the copyediting, typesetting, pagination and proofreading process, which may lead to differences between this version and the Version of Record. Please cite this article as doi: 10.1002/eji.201747450.

Keywords: Natural killer cells, CD56, Proteomics, LEGENDScreen

ABBREVIATIONS

CD	Cluster of differentiation
FC	Flow cytometry
FCS	Foetal calf serum
Grz	Granzyme
IFN-γ	Interferon-gamma
IL	Interleukin
ILC	Innate-lymphoid cell
iTRAQ	isobaric Tags for Relative and Absolute Quantification
Log_2RF	Logarithmic regulation factor
MAD	Median absolute deviation
ML12A	Myosin regulatory light chain 12a
MS	Mass spectrometry
NCR	Natural cytotoxicity receptor
NK	Natural killer

PCA	Principal component analysis
PBMC	Peripheral blood mononuclear cells
PERM	Myeloperoxidase
SPHM	N-sulphoglucosamine sulphohydrolase
TNF	Tumour necrosis factor
TPD52	Tumour protein D52

ABSTRACT

NK cells lacking CD56 ($CD56^{neg}$) were first identified in chronic HIV-1 infection. However, $CD56^{neg}$ NK cells also exist in healthy individuals, albeit in significantly lower numbers. Here, we provide an extensive proteomic characterisation of human $CD56^{neg}$ peripheral blood NK cells of healthy donors and compare them to their $CD56^{dim}$ and $CD56^{bright}$ counterparts. Unbiased large-scale surface receptor profiling clustered $CD56^{neg}$ cells as part of the main NK cell compartment and indicated an overall $CD56^{dim}$-like phenotype. Total proteome analyses of $CD56^{neg}$ NK cells further confirmed their similarity with $CD56^{dim}$ NK cells, and revealed a complete cytolytic inventory with high levels of perforin and granzyme H and M. In the present study, twelve proteins discriminated $CD56^{neg}$ NK cells from $CD56^{dim}$ NK cells with nine up-regulated and three down-regulated protein-functions in the $CD56^{neg}$ NK cell population. Those proteins were functionally related to lytic granule composition and transport, interaction with the extracellular matrix, DNA transcription or repair, and proliferation. Corroborating these results, $CD56^{neg}$ NK cells showed modest cytotoxicity, degranulation, and IFN-ɣ secretion as compared to $CD56^{dim}$ NK cells. In conclusion, $CD56^{neg}$

NK cells constitute functionally competent cells sharing many features of *bona fide* CD56^{dim} NK cells in healthy individuals, but with some distinct characteristics.

CD56 negative NK cells are under debate in patients with chronic viral infection. Here, we have now defined their molecular phenotype in healthy individuals. Extensive proteome data revealed the closest relation of CD56^{neg} to CD56^{dim} NK cells and, in parallel, confirmed their functional distinctness in activation and lytic granule pathways.

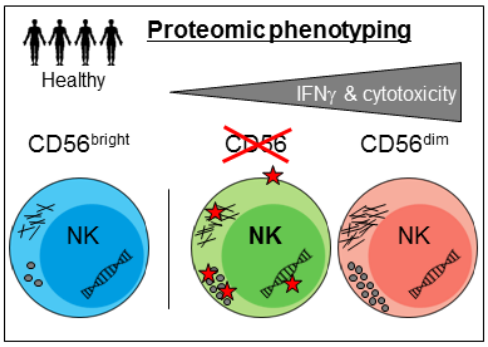

INTRODUCTION

Surface expression intensities of CD56 discriminate functionally distinct NK cell subsets, including the immune-modulatory CD56^{bright} NK cells and the major cytotoxic CD56^{dim} NK cell subset [1]. Unconventional CD56^{negative} (CD56^{neg}) NK cells were first discovered in 1995 but

their overall characteristics and function have remained elusive [2],[3]. In healthy individuals, the CD56^{neg} NK cell subset encompasses only a small proportion of the NK cell compartment in peripheral blood [4]–[7]. Functional *in vitro* studies of CD56^{neg} NK cells have suggested limited perforin expression and anti-viral activity in healthy donors [4],[8],[9].

CD56^{neg} NK cell subsets expand significantly during chronic HIV-1 and HCV infections, constituting up to half of the peripheral NK cell population at the expense of the CD56^{dim} NK cell subset [5],[10],[11]. In the case of these chronic infections, the CD56^{neg} NK cell population displays an exhausted phenotype, with reduced levels of perforin, granzyme B, IFN-ɣ, and TNF, and a lower capacity to perform cellular cytotoxicity as compared to CD56^{dim} NK cells [2],[3],[8],[11],[12]. It is unclear to what extent these expanded CD56^{neg} NK cells represent a similar or distinct phenotype as compared to CD56^{neg} NK cells in healthy individuals.

Given the limited understanding of CD56^{neg} NK cells in healthy individuals, we here carried out a detailed proteomic characterisation of CD56^{neg} NK cells in comparison to conventional CD56^{dim} and CD56^{bright} NK cells. An extensive unbiased surface receptor screen and a global proteome analysis were performed to gain detailed molecular and phenotypic information of the CD56^{neg} NK cell subset in healthy humans. This approach revealed that CD56^{neg} NK cells have a surface and total proteome related to, but not identical with, CD56^{dim} NK cells, including high expression of the cytolytic effector proteins perforin and granzyme H and M. Interestingly, a set of twelve proteins were differentially expressed as compared to CD56^{dim} NK cells, and this included reduced expression of N-sulpho-glucosamine sulphohydrolase, tumour protein D52, and myosin regulatory light chain 12A. These proteins may belong to a regulatory network controlling cytotoxic effector capacities. Functional studies examining cytotoxicity, degranulation, and IFN-ɣ production of CD56^{neg} NK cells from healthy individuals confirmed their moderate responsiveness *in vitro*.

RESULTS

Surface receptor and transcription factor profile assigns CD56^{neg} cells to the NK cell compartment

CD56^{neg} NK cells in healthy human blood donors were defined as positive for CD7 and negative for CD3, CD14, CD19 and CD56. The CD56^{neg} NK cells were positive for NKp46, EOMES, and T-bet, similar to CD56^{dim} and CD56^{bright} NK cells (Fig. 1A). With respect to expression levels of these three markers, CD56^{neg} NK cells were most similar to the CD56^{dim} NK cell subset. To further investigate the relatedness of CD56^{neg} NK cells to the other NK cell subsets, we next determined the phenotype of this population from healthy individuals using an extensive and unbiased surface receptor screen (LEGENDScreen™ by BioLegend). Lymphocytes of three healthy donors (H1-H3) were isolated and the percentage expression of surface markers was assessed based upon an internal negative control (Supporting Information file 1). In total, the expression pattern of 321 surface proteins of all three NK cell subsets (CD56^{bright}, CD56^{dim} and CD56^{neg}), T cells, and the non-NK non-T cell lymphocyte population ("dump") were analysed (Supporting Information Fig. 1). The majority of surface proteins analysed (n=245) were found to be either homogeneously expressed on all cells (n=42), have a high expression on the 'Dump' population with intermittent expression on cells of interest (n=30), or displayed undetectable expression on all cells (n=173). These, together with the lineage markers (CD3, CD14, CD19, CD123, BDCA2, FcER1a, SLAN, CD7, and CD56), were used in subsequent unbiased cluster analyses, where we focused on the 77 differentially expressed surface markers. Ward's clustering of surface receptor expression data robustly grouped the three NK cell subsets together (Fig. 1B, C), whereas deviating receptor profiles distinguished the NK compartment from T cells

and the non-NK non-T cell population as expected. Characteristic markers expressed at high levels by all three NK cell subsets included CD11b, DNAM1, 2B4, CXCR1, B7-H1, CD43, Siglec-7, CD49e, NKp80 and CD94. In conclusion, transcription factor and surface receptor expression profiles confirmed $CD56^{neg}$ NK cells as part of the NK cell compartment and suggested a marked phenotypic relation to $CD56^{dim}$ cells.

Surface receptor profiling indicate a $CD56^{dim}$-related but distinct phenotype of $CD56^{neg}$ NK cells

We next compared the surface receptor repertoire of $CD56^{neg}$ NK cells with that of the two conventional NK cell subsets ($CD56^{bright}$ and $CD56^{dim}$) to define subset-specific characteristics. In this setup, Ward's clustering included the 57 surface receptors differentially expressed in the NK cell compartment (Supporting Information Fig. 2). Again, cluster analyses confirmed highly similar surface receptor expression profiles for $CD56^{neg}$ and $CD56^{dim}$ NK cells, supported by a PCA analysis correlation value of $C_{CD56neg/dim} = 0.9207$ between $CD56^{neg}$ and $CD56^{dim}$ NK cells (Fig. 1D). The two of the most apparent phenotypic similarities that $CD56^{dim}$ and $CD56^{neg}$ NK cells consistently expressed were CD6 and CX3CR1, whereas $CD56^{bright}$ NK cells expressed low levels of these surface proteins (red in green triangles, Fig. 1C; downwards triangles yellow, Supporting Information Fig. 2. Interestingly, both proteins suggest a similar capacity of $CD56^{dim}$ and $CD56^{neg}$ cells for certain types of contact-dependent communication with other lymphocytes. CD6 contributes to the stability of immunological synapses (IS) [13] and CX3CL1, the ligand of CX3CR1, was shown to be involved in cytoskeletal reorganization and activation during crosstalk between NK cells and dendritic cells (DCs) [14]. In contrast, CD33 (Siglec-3), CD26 (dipeptidylpeptidase 4), CD27, and CD218 (IL-18R-α, interleukin-18 receptor alpha chain)

were expressed at high levels in CD56^{bright} NK cells, but only in moderate to low levels in CD56^{dim} and CD56^{neg} NK cells (blue triangles, Fig. 1C).

Beside notable similarities between CD56^{neg} and CD56^{dim} NK cells, some receptors were found differentially expressed in those two subsets. For instance, CD56^{dim} NK cells showed high levels of FcRL6 (Fc receptor-like protein 6) and CD319 (CD2-like receptor activating cytotoxic cells, CRACC), whereas CD56^{neg} NK cells displayed significantly lower levels of those receptors (red triangles, Fig. 1C). Additionally, CD127 (interleukin-7 receptor alpha chain, IL-7R-α) and CD172γ (signal-regulatory protein gamma, SIRP-γ) were more highly expressed in CD56^{neg} NK cells as compared to CD56^{dim} NK cells, which were almost negative for these two surface receptors (green triangles, Fig. 1 C). In summary, surface receptor profiling confirmed a CD56^{dim}-related, but still fairly distinct phenotype of CD56^{neg} NK cells with higher levels of CD127 and CD172γ.

Pathway analysis indicates reduced degradation of glycosaminoglycans in CD56^{neg} NK cells

To complement the results on the CD56^{dim} NK cell-related, but still distinct, phenotype of CD56^{neg} NK cells, we examined their functional protein inventory in comparison to conventional NK cell subsets by proteomics. For this purpose, the three human NK cell subsets were FACS sorted from four individual healthy donors (H4-H7), subset-specific proteins were differentially labelled (iTRAQ™ technology), and finally the population samples were combined and subjected to comparative and quantitative peptide sequencing by LC-MS (Fig. 2A). The relative abundance of peptides and corresponding proteins were calculated by comparing iTRAQ signals from two individual subsets (e.g., CD56^{neg} versus CD56^{dim} NK cells), and analysed donor-dependently using heat maps (Supporting

Information Fig. 3). In general, consistent protein abundances for the NK cell subsets in all donors were observed, and protein regulations were found in ranges described before for $CD56^{dim}$ and $CD56^{bright}$ NK cells [15]. Only donor six (H6) showed a notable variation that we however did not exclude since this donor was classified by the same criteria as the other healthy donors. Donor variations were also apparent on the level of relative regulatory information. Pearson correlation coefficients between individual donors were rather low when all characterised proteins were included in the analysis (0.31-0.62 for $CD56^{dim}/CD56^{bright}$, 0.18-0.51 for $CD56^{neg}/CD56^{bright}$, 0.16-0.57 for $CD56^{neg}/CD56^{dim}$ NK cells). However, focus on the top 50% regulated proteins in each donor increased the correlation coefficients to 0.59-0.9 for $CD56^{dim}/CD56^{bright}$, 0.45-0.83 for $CD56^{neg}/CD56^{bright}$ and 0.47-0.92 for $CD56^{neg}/CD56^{dim}$ NK cells indicating lower donor-variations of subset-specific proteins (Supporting Information Fig. 4).

Donor-specific proteomics of all three NK cell subsets contributed towards the characterisation of 3,740 proteins in total (Supporting Information Table 2). Thereby, mass spectrometric data revealed differences in the number of proteins that could be unambiguously characterised per donor (ranging from 773 to 3421 proteins in H4-H7, see Supporting Information Table 5). These data significantly complement data of our surface screen as expected. Taking proteins into account, which were identified in at least three donors, 22 surface proteins were detected with comparable results by both technologies. In general, donor-specific patterns revealed a higher dynamic range of differential protein abundances when comparing $CD56^{neg/dim}$ or $CD56^{dim/bright}$, than when comparing $CD56^{neg/bright}$ NK cells (Supporting Information Fig. 5). Thus, the $CD56^{dim}$ NK cell proteome showed the highest plasticity among the three investigated NK cell subsets.

Next, we asked whether specific cellular pathways might be differentially expressed in the three NK cell subsets. Comparative analyses of functional protein networks

(CD56$^{neg/dim}$, CD56$^{dim/bright}$, CD56$^{neg/bright}$) were performed with the support of the annotation tool DAVID using the top 10% of differentially regulated proteins from each subset comparison (median of common proteins from four donors). Interestingly, network analyses revealed an enrichment of regulated proteins in pathways playing an important role in NK cell immunity, including adhesion, activation, lytic granule transport, and cytoskeletal rearrangement processes (Fig. 2B, Supporting Information Table 3). With respect to the different NK cell subsets, those regulated pathways could be classified in three groups. The first group was found differentially regulated between the three subsets and included endocytosis and actin cytoskeleton dynamics, which were more highly expressed in CD56^{dim} NK cells (CD56^{dim} > CD56^{neg} > CD56^{bright}). The second group included pathways being differentially regulated only in comparison to CD56^{bright} NK cells (NK mediated cytotoxicity, activation signalling, focal adhesion, leukocyte transendothelial migration, FcγR-mediated phagocytosis). This further substantiates the close relation between CD56^{dim} and CD56^{neg} NK cells. The third group segregated CD56^{neg} from CD56^{dim} NK cells and defined notable differences in lysosomal dynamics and as part of this, particularly in the degradation of glycosaminoglycan. Thus, a reduced expression of components in this pathway was detected for both CD56^{neg} and CD56^{bright} as compared to the CD56^{dim} NK cell subset.

Taken together, network analyses of subset-specific regulated proteins confirmed a high degree of similarity between CD56^{dim} and CD56^{neg} NK cells. However, these analyses also suggested a lower functional responsiveness of the CD56^{neg} NK cells subset in comparison to CD56^{dim} NK cells based on lower expression of pathways involved in endosome and cytoskeleton dynamics and, in particular, indicated their limited ability to degrade glycosaminoglycans playing an important role in receptor recycling and activation.

The subset-specific functional inventory of CD56^{neg} NK cells

Surface receptor profiling and pathway analyses of proteomic data consistently suggested a CD56^{dim}-related phenotype of CD56^{neg} NK cells in healthy individuals. In parallel, these studies revealed some notable differences between CD56^{neg} and CD56^{dim} NK cells. Therefore, we next evaluated the proteomic data for proteins regulated in a subset-specific and donor-independent manner. For this analysis, we considered consistently regulated proteins detected in at least three of four donors. Furthermore, we calculated the median absolute deviation (MAD) for each protein, representing the degree of donor dependent variations. Donor-independent and subset-specific regulated proteins could be defined by low MAD values (<1.3 for CD56$^{neg/dim}$ and CD56$^{dim/bright}$; <0.7 for CD56$^{neg/bright}$), resulting in the identification of 76 proteins in the CD56$^{dim/bright}$ comparison, 57 proteins in the CD56$^{neg/bright}$ comparison, and a more limited set of twelve proteins when comparing CD56^{neg} and CD56^{dim} NK cells (Fig. 2C, Supporting Information Table 4). Thus, the CD56^{dim}-like, but functionally distinct phenotype of CD56^{neg} NK cells was found associated with a limited number of differentially abundant proteins.

Among the 12 proteins that discriminate CD56^{neg} from CD56^{dim} NK cells, we identified nine up-regulated and three down-regulated proteins in CD56^{neg} NK cells (Table 1). Four of those proteins were functionally related to lytic granule composition and transport, and included granzyme (Grz) H and M, myosin regulatory light chain 12a (ML12A), and tumour protein D52 (TPD52). Others are known to be important for the interaction with the extracellular matrix such as periostin (POSTN) and cartilage oligomeric matrix protein (COMP), for DNA transcription or repair, e.g. high mobility group protein B2 (HMGB2) and poly [ADP-ribose] polymerase 1 (PARP1), for DNA replication, like the licensing factor MCM5 (MCM5), or for cell proliferation, e.g. heterochromatin protein 1-binding protein 3 (HP1B3). Two were found associated with NK cells for the first time, namely

myeloperoxidase (PERM) and N-sulphoglucosamine sulphohydrolase (SPHM). Myeloperoxidase is a lysosomal protein that here most significantly discriminated $CD56^{neg}$ and $CD56^{dim}$ NK cells. It was most highly expressed in $CD56^{neg}$, moderately in $CD56^{bright}$, and low in $CD56^{dim}$ NK cells. Interestingly, GrzH and GrzM were expressed with donor-independent and superior levels in $CD56^{neg}$ NK cells, and the other granzymes showed similar but less robust up-regulation as compared to $CD56^{dim}$ NK cells (Table 2). Likewise, perforin was detected in $CD56^{neg}$ NK cells at levels that even slightly exceeded those in the $CD56^{dim}$ subset in individual donors. On the other hand, we identified only three donor-independently down-regulated proteins discriminating $CD56^{neg}$ from $CD56^{dim}$ NK cells. First, myosin regulatory light chain 12a and tumour protein D52 that both can contribute to lytic vesicle trafficking in NK cells, potentially in line with more limited degranulation and cytotoxic capacities of $CD56^{neg}$ NK cells. Second, the lysosomal sulfatase N-sulphoglucosamine sulphohydrolase, which supports receptor signalling, was significantly less abundant in $CD56^{neg}$ than in the $CD56^{dim}$ NK cells.

In conclusion, the total proteome data complemented the initial surface receptor screen and allowed us to establish a first model of the functional inventories that characterise the distinct phenotypes of the three human NK subsets (Fig. 3). This model integrates data from both the surface receptor screen and the total cellular proteomics. Besides the comparative view on subset-specific NK cell receptor markers, this model illustrates the phenotypic relation in terms of differences and similarities of the three human NK cell subsets. Notable similarities between $CD56^{neg}$ and $CD56^{dim}$ NK cells in comparison to $CD56^{bright}$ NK cells were detected in all processes, i.e. adhesion (high for filamin-A, calpain-2, SH3K1 and vinculin, low for CAPG), IS/cytotoxicity (e.g. high for S100A4, phostensin, annexin A4 and CLIC3 and low for COTL), activation (e.g. high for GRAP2, CD3ζ, PTCA, FcεRɣ), as well as for the content of lytic granules (e.g., high for perforin, low

for GrzK). However, the model also underscores a CD56^{neg} NK cell-specific phenotype apparent by their distinct expression of adhesive capacities (high for COMP and POSTN).

CD56^{neg} NK cells in healthy human donors have lower functional capacity compared to CD56^{dim} NK cells

To investigate whether the CD56^{neg} NK cell population was able to use the cytolytic inventory effectively, we analysed the following NK cell effector functions: degranulation, IFN-γ production, as well as cytotoxic capacity. NK cell responsiveness studies were performed using FACS-sorted NK cell subsets isolated from peripheral blood of healthy human donors. First, CD56^{neg}, CD56^{bright}, and CD56^{dim} NK cells were sorted and activated with IL-12/15/18, K562, or a combination of both. NK cell subset degranulation was measured as CD107a surface accumulation by flow cytometry. In general, the CD56^{dim} NK cell population showed the highest degranulation rates for all stimulations, followed by CD56^{neg} and CD56^{bright} NK cells. Notably, exposure to K562 target cells alone or in combination with the interleukin cocktail increased the frequency of CD107a-expressing CD56^{neg} NK cells (Fig. 4A), but it still remained significantly lower compared to the CD56^{dim} NK cell subset. Next, IFN-ɣ levels were analysed in the subsets. As expected, cytokine stimulation most efficiently activated IFN-ɣ release in the immune-modulatory CD56^{bright} NK cells in all donors. CD56^{neg} NK cells exhibited relatively low IFN-ɣ levels in unstimulated samples, and expression was induced in all tested activating conditions. Co-activation by cytokines and K562 target cells had a positive synergistic effect likewise in the other two subsets (Fig. 4B). Finally, the cytotoxic capacity of the sorted primary NK cell subsets was measured as the capacity to lyse CFSE-labelled K562 target cells. In line with the slightly lower degranulation levels detected, CD56^{neg} NK cells had a lower cytotoxic capacity as compared to CD56^{dim} NK cells (Fig. 4C).

In summary, these results show that the CD56^{neg} NK cell subset can respond with known NK cell functions upon stimulation. However, under the *in vitro* conditions tested in this study, CD56^{neg} NK cells from healthy individuals exhibited a moderate reduction in killing capacity, degranulation, and IFN-ɣ production in comparison to CD56^{dim} NK cells.

DISCUSSION

CD56^{neg} NK cells expand, sometimes to a remarkably large population, in patients with chronic viral infections [3]. However, a CD56^{neg} NK cell population is also detectable in much smaller numbers in the blood of healthy humans. In this study, we have characterised this subset of NK cells in healthy individuals focusing on their functional inventory, which we profiled in comparison to CD56^{dim} and CD56^{bright} NK cells.

The CD56^{neg} NK cell population investigated in this study presented with an NKp46^{pos}EOMES^{pos}T-bet^{high} phenotype in all healthy donors. This, together with data from receptor profiling as well as proteomics, indicate that this subset is in many respects similar to CD56^{dim} NK cells. For instance, CD56^{neg} and CD56^{dim} NK cells were characterised by similar high expression of CD6 and CX3CR1. CD6 contributes to cytokine and chemokine secretion (IFN-ɣ, TNF, CXCL10/IP-10, CXCL1) in CD56^{dim} NK cells suggesting a similar role in CD56^{neg} NK cells [16]. Interestingly, in T cells, CD6 stabilizes the immunological synapse in crosstalk with DCs [17],[18]. Since the crosstalk between NK cells and DCs also depends on stable immunological synapses, one might speculate on a crucial role for CD6 also in CD56$^{dim/neg}$ NK cell function [19]. In line with this, CX3CR1, via its interaction with CX3CL1 on DCs, might support CD56^{neg} NK cell activation and IFN-ɣ production, as previously shown for conventional NK cells [14]. In contrast to these similarly expressed receptors, expression of CD127 (IL-7R-α) and CD172ɣ (SIRP-ɣ) on CD56^{neg} NK cells robustly segregate them from

CD56^{dim} NK cells. CD127 serves as the receptor for IL-7 and thymic stromal lymphopoietin (TSLP) [20], and its expression in CD56^{neg} NK cells suggests this subset may be similar to murine IL-7-dependent thymus-derived NK cells which have limited cytotoxicity [21],[22]. However, the limited cytotoxicity reported for this subset in the murine system was accompanied with higher IFN-γ response, a pattern we did not observe for the human CD56^{neg} population (Fig. 4B). CD172γ belongs to the signal regulatory protein (SIRP) receptor family, contributes to adhesion and transendothelial migration in T cells [23], but its function is relatively little studied in NK cells. Interestingly, SIRP receptors are considered negative regulators for tyrosine kinase signalling and an engagement of SIRP-α by CD47 was shown to limit NK cell cytotoxicity [24].

With respect to their donor-independent and subset-specific inventory, CD56^{neg} NK cells were found to be well equipped for performing cellular cytotoxicity. While expression of GrzA was previously reported for the CD56^{neg} population [4],[9], we here characterised expression patterns of all five granzymes. Interestingly, GrzH and M were detected with the highest abundance in CD56^{neg} as compared to CD56^{dim} and CD56^{bright} NK cells. Perforin was detected at high levels by proteomics in both the CD56^{neg} NK cell subset and in the CD56^{dim} NK cells (CD56^{neg}~CD56^{dim}>CD56^{bright}). Flow cytometry confirmed this result, but in addition indicated slightly lower perforin levels in CD56^{neg} NK cells (Supporting Information Fig. 6). A possible explanation for these somewhat divergent findings might be found in the fine specificity of the antibodies used for flow cytometry, which detect active granule-associated perforin but likely not all other modified or immature perforin variants.

However, despite their cytolytic inventory, CD56^{neg} NK cells were less responsive after stimulation with K562 cells than CD56^{dim} NK cells, as shown by lower target cell killing rate, lower frequency of degranulation, and less IFN-ɣ production. The frequency of IFN-ɣ-

producing CD56^{neg} NK cells in response to IL-12/15/18 stimulation resembled that of CD56^{dim} NK cells and was inferior to that of CD56^{bright} NK cells. Interestingly, the lowest IFN-γ expression levels observed here in response to K562 cells are fully in accordance with the study by Milush et al., whereas the lower degranulation rate is contradicting [4]. Notably, the three NK cell subsets were first sorted from PBMCs, in contrast to Milush et al., who monitored those as part of total PBMCs. Hence, a lower degranulation and killing capacity of CD56^{neg} NK cells *in vitro* is part of their phenotype in healthy individuals.

To what extent CD56^{neg} NK cells can use their cytolytic potential during viral infection is of central interest. The molecular phenotyping performed in this study cannot give a complete answer, but indicates a small regulatory network and two principal mechanisms: The first indicates the importance of cellular adhesion. Interestingly, CD56^{neg} NK cells were reported to be less motile, remain longer in arrest, and show decreased Ca^{2+}- and pTyr-levels [25]. Hence, expression of CD56 appears to correlate with adhesion and responsiveness. Here, we now complement with data on adhesion-related proteins that were found with higher expression levels in CD56^{neg} compared to CD56^{dim} (COMP, POSTN, SIRP-γ) or CD56^{bright} NK cells (CAN2, FLNA, SH3K1, VINC). Thus, these components likely contribute to the arrest and motility phenotype of CD56^{neg} NK, which in turn limits their responsiveness.

The second principal mechanism seems to be the control of component activities at the NK cell immunological synapse. Only three proteins were found donor-independently less expressed in CD56^{neg} NK cells as compared to cytotoxic CD56^{dim} NK cells, namely SPHM, ML12A, and TD52. SPHM is part of the glycosaminoglycan degradation pathway, which proteomics identified by network analyses (Fig. 2B). In particular, SPHM acts as a lysosomal heparan sulphate (HS) sulphatase [26], which supports HS degradation and in

parallel might regulate its interaction with the natural cytotoxicity receptors (NCRs) NKp30, NKp44, and NKp46 [27],[28], as well as with KIR2DL4 [29]. Importantly, HS is able to significantly modulate NCR-mediated signalling and consequently affect NK cell activation and cytotoxicity [30],[31]. Low SPHM levels in $CD56^{neg}$ NK cells might increase HS availability, leading to elevated blocking of the NCRs, which may also contribute to their low responsiveness. Future studies should analyse HS levels in all three NK cell subsets to clarify the potential relevance of SPHM and HS-related mechanisms for NK cell effector functions. ML12A and TPD52 have not been previously studied in NK cells. However, both proteins are involved in receptor and vesicle trafficking processes, which are important functions for NK cell cytotoxicity. ML12A maintains the stability of myosin IIa [32], which is a key player in NK cell biology. This actin-binding protein guides lytic granules through the dense F-actin mesh to the NK-IS and promotes lytic granule secretion [33]–[35]. Interestingly, TPD52 might be required for efficient lytic granule secretion as well. TPD52 was shown to mediate lytic granule (LAMP1) accumulation at the plasma membrane of non-NK cells in a Ca^{2+} dependent process [36]. Thus, lower expression of ML12A and TPD52 may help explain a reduced degranulation and cytolytic capacity of $CD56^{neg}$ NK cells. One may speculate that lytic vesicles are differentially active in $CD56^{neg}$ NK cells. Besides unique profiles of GrzM and K, mass spectrometry identified the lysosomal oxidase PERM with higher abundance in $CD56^{neg}$ NK cells ($CD56^{neg}$>$CD56^{bright}$>$CD56^{dim}$, Table 2). Secreted PERM has been shown to have pro-inflammatory effects on neutrophil extravasation whereas intracellular PERM is involved in the regulation of protease processing and might be a regulator for granzyme activity in lytic granules [37]. Together, this indicates a possible role of PERM in regulation of responsiveness and effector function in $CD56^{neg}$ NK cells.

In conclusion, a combination of surface receptor screen and proteomics was employed here to establish a detailed model of the donor-independent functional inventory of

CD56^{neg} NK cells in healthy individuals (Fig. 3). With these results, CD56^{neg} NK cells are now better defined as a member of the NK cell compartment, and their intermediate responsiveness in comparison to the conventional NK cell subsets can be rationalized by a limited set of subset-specific protein functions. These functions suggest unique adhesion and activation properties. Future studies should aim to ascertain whether the CD56^{neg} NK cells here characterised in detail in healthy donors are similar to those seen expanded in humans with HIV-1 or HCV infection. It is possible that such comparisons can advise ways to exploit or manipulate this subset in infected individuals.

MATERIALs and METHODS

Human blood samples

For surface receptor screening, peripheral blood samples were collected from healthy individuals recruited at the Blood Transfusion Clinic at the Karolinska University Hospital Huddinge. Written informed consent was obtained from all the donors in accordance with study protocols conforming to the provisions of the Declaration of Helsinki and approved by the Regional Ethics Review Board in Stockholm. For proteome analyses and functional assays, buffy coats from blood donations of healthy human volunteers who provided informed consent were obtained from the Institute for Clinical Transfusion Medicine, Klinikum Braunschweig, Germany. Blood donors' health is rigorously checked before being admitted for blood donation. This process included a national standardized questionnaire with health questions, an interview with a medical doctor and standardized laboratory tests for a) infections HIV1/2, HBV, HCV, Syphilis (serology and/or nucleic acid testing) and b) haematological cell counts. Buffy coats were produced from whole blood donations on day 1 by using the Top & Bottom Extraction Bag System (Polymed Medical Devices^{TM}, Triple

Blood Bag System, No. 7300; containing CPDA-1). PBMCs were isolated by Biocoll density gradient centrifugation (Biochrome AG) on day 2. PBMCs were cultured overnight in RPMI-1640 medium (GIBCO) supplemented with 10% foetal bovine serum (FBS) gold (PAA Laboratories, Etobicoke, ON, Canada), 2 mM L-glutamine (Invitrogen), 50 units/ml penicillin, 50 µg/ml streptomycin (Gibco), and 50 U IL-2/ml (PeproTech) at 37°C in a humid 7.5% CO_2 atmosphere.

Staining and sorting of primary human NK cells

The surface receptor screen was performed using the LEGENDScreen™ kit from Biolegend as previously described [38]. PBMCs from buffy coats of three healthy donors (H1-H3) were isolated by density centrifugation and cultured overnight. Cells were subsequently stained with an antibody panel designed to exclude myeloid, B, DC and T cells. We used CD3, CD14 and CD19 and additionally CD20, CD123, BDCA2, FcEr1a and SLAN as negative markers. As positive selection markers we used CD56 and CD7. The detailed gating strategy is described in Supporting Information Fig. 7A. PBMCs were first pre-stained with the antibodies of interest and then added to each well of the plates in the LEGENDScreen™ kit. Each staining step was performed at 4°C for 20 minutes. Cells were washed and fixed for 10 minutes using BD cell fix prior to running on a BD LSRFortessa.

Semi-quantitative total proteome analysis utilizing MS was performed on the three NK cell subsets derived from four healthy individuals (H4-H7). PBMCs were FACS-based sorted using the Aria-II SORP, for which PBMCs were cultured overnight, washed, stained with antibodies for 15 minutes at 4°C, washed and then immediately sorted. We used CD3, CD14 and CD19 for excluding T, Dendritic and B cells, and non-activated NK cell subset were positively selected by CD7, CD56 and CD16 expressions. The gating strategy is described in

Supporting Information Fig. 7B. Cell purities and yields of sorted $CD56^{bright}$ $CD16^{-}$ ('$CD56^{bright}$'), $CD56^{dim}$ $CD16^{+}$ ('$CD56^{dim}$') and $CD56^{neg}$ $CD16^{+}$ ('$CD56^{neg}$') cells are listed in Supporting Information Table 5. Sorted cells were pelleted and stored at -80°C until proteome analysis. Additional subsequent flow cytometric analyses of PMBCs for intracellular perforin and CD56 as well as for intranuclear T-bet and EOMES and surface NKp46 expression were performed on a BD LSR-II SORP using the same antibodies and gating strategy to identify NK cell subsets as for NK cell sorting for the total proteome analysis.

For the LEGENDScreen the following monoclonal antibodies were used: anti-CD14-FITC (Dako, clone TÜK4, Cat: F0844), anti-FcεR1α-FITC (Biolegend, clone AER-37, Cat: 334608), anti-SLAN-FITC (Miltenyi Biotec, 130-099-128, Cat: DD-1), anti-CD123-FITC (Biolegend, clone 6H6, Cat: 306013), anti-CD20-FITC (Biolegend, clone 2H7, Cat: 302303), anti-CD19-FITC (BD, clone HIB19, Cat: 555412), anti-BDCA2-FITC (Miltenyi Biotec, clone AC144, Cat: 130-090-510), anti-CD7-A700 (eBioscience, clone eBio124-1D1, Cat: 56-0079-42), anti-CD3-BV785 (Biolegend, clone OKT3, Cat: 317329), anti-CD56-ECD (Beckman Coulter, clone N901, Cat: A82943).

For NK cell isolation for the total proteome analysis and functional assays as well as additional flow cytometric analyses the following monoclonal antibodies were used: anti-CD3-FITC (BD, clone UCHT1, Cat: 555916), anti-CD7-PE (eBioscience, clone eBio124-1D1, Cat: 12-0079-42), anti-CD14-FITC (BD, clone M5E2, Cat: 555397), anti-CD16-BV421 (BD, clone 3G8, Cat: 562874), anti-CD19-FITC (BD, clone HIB19, Cat: 555412), anti-CD56-APC (Miltenyi, clone REA196, Cat: 130-100-698), anti-CD335-PE-Cy7 (anti-NKp46) (Biolegend, clone 9E2, Cat: 331915), anti-T-bet-BV605 (Biolegend, clone 4B10, Cat: 644817), anti-EOMES-PE-Cy7 (eBioscience, clone WD1928, Cat: 25-4877-41), anti-perforin-PE-Cy7

(Biolegend, clone dG9, Cat: 308125), anti-perforin-PE-Cy7 (Biolegend, clone D48, Cat: 353315).

LC-MS/MS-based total proteome analysis

Further processing of NK cell subsets for total proteome analysis is graphically summarized in Figure 2A. Material was processed and analysed as described by *Scheiter et al.*[15], with slight modifications. Briefly, thawed sorted cells were lysed, dodecyl-β-D-maltoside (DDM) (Carl Roth, Germany) served as a surfactant in the lysis buffer. Proteins were precipitated and digested. Tryptic peptides were labelled with isobaric iTRAQ reagents (Applied Biosystems) for subset-specific MS identification. For NK cells from four donors with sufficiently high numbers of $CD56^{neg}$ cells (>$3.5x10^5$ cells), MS data was obtained individually. Equal amounts of labelled peptides from $CD56^{bright}$, $CD56^{dim}$ and $CD56^{neg}$ NK cells were combined, fractionated by strong cation exchange chromatography (SCX) and sequenced with an UltiMate 3000 RSLCnano LC system (Thermo Scientific) connected to an LTQ Orbitrap Fusion Tribrid Fourier transform mass spectrometer (Thermo Scientific). Identification and relative quantification of peptides and corresponding proteins from MS/MS raw data was performed with Proteome Discover (version 1.4.1.14) and Mascot Server (version 2.4.1.) based on Swiss-Prot protein database (released in January 2014, taxonomy Homo sapiens). The log_2 normalized regulation factors (RF), based on individual iTRAQ label intensity of unique peptides, represent the relative abundance of a protein in $CD56^{dim}$ compared to $CD56^{bright}$ (RF = $CD56^{dim}/CD56^{bright}$), $CD56^{neg}$ compared to $CD56^{bright}$ (RF = $CD56^{neg}/CD56^{bright}$) or $CD56^{neg}$ compared to $CD56^{dim}$ (RF = $CD56^{neg}/CD56^{dim}$) NK cells.

Statistical data analysis

Analysis of the flow cytometry data for the phenotypic screen data was performed using FlowJo (Tree Star Inc.) version 9, and version 10 for other expression data. Populations required at least 100 events to be considered as robust. The resulting surface screen data was compiled in Microsoft Excel 2011, and to avoid biasing subsequent analysis, the markers used to identify the subsets in this screen, i.e. those in our staining panel, were removed. Surface screen data was then subjected to Ward's clustering and principal component analysis performed using JMP 11. Two-way ANOVA or paired t-test, each with Bonferroni-Holm correction for multiple testing, were performed for evaluation of CD56, NKp46, EOMES, T-bet, K562 lysis, CD107a and IFN-ɣ expression using GraphPad Prism version 7. Due to the small sample size of n=3 or n=4, p-values are considered as score rather than probability.

For the total proteome analysis, only proteins that were identified with a minimum of 2 unique peptides were evaluated. Subset-specifically regulated proteins were determined based on H4-H7; only proteins measured in at least 3 out of 4 replicates were assessed. To achieve discrimination despite the limited number of replicates (n=4), an estimation of the standard deviation by taking RFs of all proteins into account was performed using a model described by Klawonn [39]. Our model used the Median Absolute Deviation from the median (MAD) of all proteins as an estimator for the standard deviation of a normal distribution corrected for small sample sizes. Proteins were considered to show high donor-dependent regulation when their MAD exceeded 1.3 for $CD56^{dim}/CD56^{bright}$ and $CD56^{neg}/CD56^{dim}$, and 0.7 for $CD56^{neg}/CD56^{bright}$ (Supporting Information Fig. 8). Box-Whisker and MAD value plots were generated and Ward's hierarchical clustering was performed using R to generate heat maps allowing assessment of reproducibility for common proteins across the 4 experiments.

Analysis for enriched KEGG pathways in the group of the top 10% of regulated proteins was performed using DAVID Functional Annotation Tool (V6.8, March 2017). The median regulation factor of proteins identified in at least 3 out of the 4 donors (1669 proteins) was used.

Functional Assays

Freshly sorted NK cell subsets were used to assess NK cell effector functions, employing the same staining and gating procedure as described above for NK cell isolation. Samples were analysed on a BD LSR-II SORP flow cytometer. In the non-radioactive killing assay the capacity of NK cell subsets to induce apoptosis in K562 target cells was assessed [40]. Briefly, graded numbers of NK cell subsets were incubated with CFSE-labelled K562 cells (1x10^4, viability > 92%) at indicated E:T ratios in 100 µl total volume for 4h at 37°C, 5% CO_2. Culture medium without phenol red was used and the NK-K562 cell suspension was spun (120xg, 2 min, RT) to increase cell contact immediately prior incubation start. The different E:T ratios were mostly run at duplicates per NK cell subset. Cell viability was assessed by 7-AAD just added before analysis. Target cells were gated onto in the FSC/SSC plot and additionally identified as CFSE-positive cells. Mostly, a minimum of 3000 $CFSE^+$ target cells were counted. Frequency of apoptotic target cells was calculated as experimental lysis – spontaneous lysis using the following formula:% apoptotic target cells = ((CFSE+ 7-AAD+ cells / all CFSE+ cells) * 100) – ((CFSE+ 7-AAD+ cells / all CFSE+ cells) of the K562 only sample * 100)].

Degranulation, measured by CD107a expression, and intracellular IFN-ɣ expression of isolated NK cell subsets (1x10^4) in response to stimulation with the indicated combinations of IL-12 (10 ng/ml), IL-15 (10 ng/ml), IL-18 (100 ng/ml) and K562 (E:T 2:1) target cells were assessed after 6 h incubation at 37°C. Brefeldin A and monensin were added to the cultures after 1 h of incubation followed by 5 more hours. Each stimulation condition was measured as duplicate. Cells were stained with fixable Live/Dead (Invitrogen, Cat: L34961), anti-CD107a mAb (Biolegend, clone H4A3, Cat: 328617) and anti-IFN-*ɣ* mAb (Biolegend, clone 4S.B3, Cat: 502527) and fixed.

ACKNOWLEDGEMENTS

We thank the Blood Bank NSTOB Springe, Germany and Prof. Dr. Henk Garritsen, Klinikum Braunschweig for providing us with blood. We thank Josef Wissing, Undine Felgenträger, Reiner Munder, Kirsten Minkhart, Steffi Trittel and Peggy Riese for technical assistance and advice and Daniel Meston for proofreading. This work was realized in the frame of the International Research Training Group (IRTG1273) and funded by the DFG. Further support came from grants from the Swedish Research Council and the Swedish Cancer Society. JD was supported by Fundação para a Ciência e a Tecnologia (FCT) Doctoral Fellowship SFRH/BD/85290/2012, co-funded by the POPH-QREN and the European Social Fund (FSE).MH, LJ, NKB, HGL and JKS conceived and designed the research. LG supported the design and performed NK cell subset sorting. JD and EL optimized and performed the flow cytometry experiments of the LEGENDScreen and DM analysed the acquired data. JV designed and performed the MS-based total proteome screen and functional assays, and analysed the data. FK, DM and JV performed statistical analyses. MH, DM, JV, LJ, NKB, HGL and JKS prepared the manuscript.

CONFLICT OF INTEREST DISCLOSURE

The authors Jenny Voigt, David Malone, Joana Dias, Edwin Leeansyah, Lothar Gröbe, Niklas Björkström, Hans-Gustaf Ljunggren, Frank Klawonn, Maxi Heyner, Johan Sandberg and Lothar Jänsch declare that they have no commercial or financial conflicts of interest.

BIBLIOGRAPHY

1. **Caligiuri MA**. Human natural killer cells. *Blood*. 2008; **112**:461–469.

2. **Hu PF, Hultin LE, Hultin P, Hausner MA, Hirji K, Jewett A, Bonavida B, *et al.*** Natural killer cell immunodeficiency in HIV disease is manifest by profoundly decreased numbers of CD16+CD56+ cells and expansion of a population of CD16dimCD56- cells with low lytic activity. *J. Acquir. Immune Defic. Syndr. Hum. Retrovirol.* 1995; **10**:331–40.

3. **Björkström NK**, **Ljunggren H-G**, **Sandberg JK**. CD56 negative NK cells: origin, function, and role in chronic viral disease. *Trends Immunol.* 2010; **31**:401–6.

4. **Milush JM, López-Vergès S, York VA, Deeks SG, Martin JN, Hecht FM, Lanier LL, *et al.*** CD56 neg CD16 + NK cells are activated mature NK cells with impaired effector function during HIV-1 infection. *Retrovirology*. 2013; **10**:1–13.

5. **Eller MA, Eller LA, Ouma BJ, Thelian D, Gonzalez VD, Guwatudde D, McCutchan FE, *et al.*** Elevated natural killer cell activity despite altered functional and phenotypic profile in Ugandans with HIV-1 clade A or clade D infection. *J. Acquir. Immune Defic. Syndr.* 2009; **51**:380–9.

6. **Hong HS, Eberhard JM, Keudel P, Bollmann BA, Ahmad F, Ballmaier M, Bhatnagar N, *et al.*** Phenotypically and functionally distinct subsets contribute to the expansion of CD56-/CD16+ natural killer cells in HIV infection. *AIDS*. 2010; **24**:1823–34.

7. **Mavilio D, Lombardo G, Benjamin J, Kim D, Follman D, Marcenaro E, Shea MAO, *et al.*** Characterization of CD56-/CD16+ natural killer (NK) cells : A highly dysfunctional NK subset expanded in HIV-infected viremic individuals. *Proc. Natl. Acad. Sci.* 2005; **102**:2886–2891.

8. **Gonzalez VD, Falconer K, Björkström NK, Blom KG, Weiland O, Ljunggren HG, Alaeus A, *et al.*** Expansion of functionally skewed CD56-negative NK cells in chronic hepatitis C virus infection: correlation with outcome of pegylated IFN-alpha and ribavirin treatment. *J. Immunol.* 2009; **183**:6612–8.

9. **Jacobson A**, **Bell F**, **Lejarcegui N**, **Mitchell C**, **Frenkel L**, **Horton H**. Healthy Neonates Possess a CD56-Negative NK Cell Population with Reduced Anti-Viral Activity. *PLoS One*. 2013; **8**:e67700.

10. **Mavilio D, Benjamin J, Daucher M, Lombardo G, Kottilil S, Planta MA, Marcenaro E, *et al.*** Natural killer cells in HIV-1 infection: dichotomous effects of viremia on inhibitory and activating receptors and their functional correlates. *Proc. Natl. Acad. Sci. U. S. A.* 2003; **100**:15011–6.

11. **Alter G, Teigen N, Davis BT, Addo MM, Suscovich TJ, Waring MT, Streeck H, *et al.*** Sequential deregulation of NK cell subset distribution and function starting in acute HIV-1 infection. *Blood*. 2005; **106**:3366–9.

12. **Alter G, Suscovich TJ, Kleyman M, Teigen N, Streeck H, Zaman MT, Meier A, *et al.*** Low perforin and elevated SHIP-1 expression is associated with functional anergy of natural

killer cells in chronic HIV-1 infection. *AIDS*. 2006; **20**:1549–1560.

13. **Santos R**, **Oliveira L**, **Carmo A**. Tuning T Cell Activation: The Function of CD6 at the Immunological Synapse and in T Cell Responses. *Curr. Drug Targets*. 2016; **17**:630–9.

14. **Pallandre JR, Krzewski K, Bedel R, Ryffel B, Caignard A, Rohrlich PS, Pivot X, *et al.*** Dendritic cell and natural killer cell cross-talk: a pivotal role of CX3CL1 in NK cytoskeleton oragnization and activation. *Blood*. 2008; **112**:4420–4.

15. **Scheiter M, Lau U, van Ham M, Bulitta B, Gröbe L, Garritsen H, Klawonn F, *et al.*** Proteome analysis of distinct developmental stages of human natural killer (NK) cells. *Mol. Cell. Proteomics*. 2013; **12**:1099–114.

16. **Braun M, Müller B, ter Meer D, Raffegerst S, Simm B, Wilde S, Spranger S, *et al.*** The CD6 scavenger receptor is differentially expressed on a CD56 dim natural killer cell subpopulation and contributes to natural killer-derived cytokine and chemokine secretion. *J. Innate Immun.* 2011; **3**:420–434.

17. **te Riet J**, **Helenius J**, **Strohmeyer N**, **Cambi A**, **Figdor CG**, **Müller DJ**. Dynamic coupling of ALCAM to the actin cortex strengthens cell adhesion to CD6. *J. Cell Sci.* 2014; **127**:1595–606.

18. **Tudor C, te Riet J, Eich C, Harkes R, Smisdom N, Bouhuijzen Wenger J, Ameloot M, *et al.*** Syntenin-1 and ezrin proteins link activated leukocyte cell adhesion molecule to the actin cytoskeleton. *J. Biol. Chem.* 2014; **289**:13445–13460.

19. **Cooper MA**, **Fehniger TA**, **Fuchs A**, **Colonna M**, **Caligiuri MA**. NK cell and DC interactions. *Trends Immunol.* 2004; **25**:47–52.

20. **Isaksen DE**, **Baumann H**, **Zhou B**, **Nivollet S**, **Farr AG**, **Levin SD**, **Ziegler SF**.

Uncoupling of proliferation and Stat5 activation in thymic stromal lymphopoietin-mediated signal transduction. *J. Immunol.* 2002; **168**:3288–3294.

21. **Smyth MJ**, **Nutt SL**. IL-7 and the thymus dictate the NK cell 'labor market'. *Nat. Immunol.* 2006; **7**:1134–36.

22. **Vosshenrich CAJ, García-Ojeda ME, Samson-Villéger SI, Pasqualetto V, Enault L, Richard-Le Goff O, Corcuff E, *et al.*** A thymic pathway of mouse natural killer cell development characterized by expression of GATA-3 and CD127. *Nat. Immunolgoy*. 2006; **7**:1343.

23. **Stefanidakis M**, **Newton G**, **Lee WY**, **Parkos CA**, **Luscinskas FW**. Endothelial CD47 interaction with SIRP gamma is required for human T-cell transendothelial migration under shear flow conditions in vitro. *Blood*. 2008; **112**:1280–1289.

24. **Kim MJ, Lee JC, Lee JJ, Kim S, Lee SG, Park SW, Sung MW, *et al.*** Association of CD47 with natural killer cell-mediated cytotoxicity of head-and-neck squamous cell carcinoma lines. *Tumor Biol.* 2008; **29**:28–34.

25. **Mace EM**, **Gunesch JT**, **Dixon A**, **Orange JS**. Human NK cell development requires CD56-mediated motility and formation of the developmental synapse. *Nat. Commun.* 2016; **7**:12171.

26. **Sidhu NS, Schreiber K, Pröpper K, Becker S, Usón I, Sheldrick GM, Gärtner J, *et al.*** Structure of sulfamidase provides insight into the molecular pathology of mucopolysaccharidosis IIIA. *Acta Crystallogr. Sect. D Biol. Crystallogr.* 2014; **70**:1321–1335.

27. **Bloushtain N, Qimron U, Bar-Ilan A, Hershkovitz O, Fima E, Korc M, Vlodavsky I, *et al.*** Membrane-associated heparan sulfate proteoglycans are involved in the recognition of cellular targets by NKp30 and NKp46. *J. Immunol.* 2004; **173**:2392–2401.

28. **Hecht ML, Rosental B, Horlacher T, Hershkovitz O, De Paz JL, Noti C, Schauer S, *et al.*** Natural cytotoxicity receptors NKp30, NKp44 and NKp46 bind to different heparan sulfate/heparin sequences. *J. Proteome Res.* 2009; **8**:712–720.

29. **Brusilovsky M, Cordoba M, Rosental B, Hershkovitz O, Andrake MD, Pecherskaya A, Einarson MB, *et al.*** Genome-wide siRNA screen reveals a new cellular partner of NK cell receptor KIR2DL4: heparan sulfate directly modulates KIR2DL4-mediated responses. *J. Immunol.* 2013; **191**:5256–5267.

30. **Brusilovsky M**, **Radinsky O**, **Yossef R**, **Campbell KS**, **Porgador A**. Carbohydrate-mediated modulation of NK cell receptor function: structural and functional influences of heparan sulfate moieties expressed on NK cell surface. *Front. Oncol.* 2014; **4**:185.

31. **Brusilovsky M, Radinsky O, Cohen L, Yossef R, Shemesh A, Braiman A, Mandelboim O, *et al.*** Regulation of natural cytotoxicity receptors by heparan sulfate proteoglycans in -cis: A lesson from NKp44. *Eur. J. Immunol.* 2016; **45**:1180–1191.

32. **Park I, Han C, Jin S, Lee B, Choi H, Kwon JT, Kim D, *et al.*** Myosin regulatory light chains are required to maintain the stability of myosin II and cellular integrity. *Biochem. J.* 2011; **434**:171–180.

33. **Andzelm MM**, **Chen X**, **Krzewski K**, **Orange JS**, **Strominger JL**. Myosin IIA is required for cytolytic granule exocytosis in human NK cells. *J. Exp. Med.* 2007; **204**:2285–2291.

34. **Watanabe T**, **Hosoya H**, **Yonemura S**. Regulation of Myosin II Dynamics by Phosphorylation and Dephosphorylation of Its Light Chain in Epithelial Cells. *Mol. Biol. Cell*. 2007; **18**:605–616.

35. **Sanborn KB, Rak GD, Maru SY, Demers K, Difeo A, Martignetti JA, Betts MR, *et al.*** Myosin IIA associates with NK cell lytic granules to enable their interaction with F-actin and

function at the immunological synapse. *J. Immunolgy*. 2009; **182**:6969–6984.

36. **Thomas DD**, **Martin CL**, **Weng N**, **Byrne JA**, **Groblewski GE**. Tumor protein D52 expression and Ca2+-dependent phosphorylation modulates lysosomal membrane protein trafficking to the plasma membrane. *Am. J. Physiol. Cell Physiol.* 2009; **298**:725–739.

37. **Klebanoff SJ**. Myeloperoxidase: friend and foe. *J. Leukoc. Biol.* 2005; **77**:598–625.

38. **Dias J**, **Sandberg JK**, **Leeansyah E**. Extensive Phenotypic Analysis, Transcription Factor Profiling, and Effector Cytokine Production of Human MAIT Cells by Flow Cytometry. In: *Methods in molecular biology (Clifton, N.J.)*.Vol 1514.; 2017:241–256.

39. **Klawonn F.** Significance tests to identify regulated proteins based on a large number of small samples. *Kybernetica*. 2012; **48**:478–493.

40. **Park KH**, **Park H**, **Kim M**, **Kim Y**, **Han K**, **Oh EJ**. Evaluation of NK cell function by flowcytometric measurement and impedance based assay using real-time cell electronic sensing system. *Biomed Res. Int.* 2013; **2013**:210726.

41. **Eiserich J**, **Estévez A**, **Bamberg T**, **Ye Y**, **Chumley P**, **Beckman J**, **Freeman B**. Microtubule dysfunction by posttranslational nitrotyrosination of alpha-tubulin: a nitric oxide-dependent mechanism of cellular injury. *Proc. Natl. Acad. Sci. U. S. A.* 1999; **96**:6365–70.

42. **Pusterla T**, **de Marchis F**, **Palumbo R**, **Bianchi ME**. High mobility group B2 is secreted by myeloid cells and has mitogenic and chemoattractant activities similar to high mobility group B1. *Autoimmunity*. 2009; **42**:308–310.

43. **Zimmerman J**, **Maher LJ**. Transient HMGB protein interactions with B-DNA duplexes and complexes. *Biochem. Biophys. Res. Commun.* 2008; **371**:79–84.

44. **Masuoka M, Shiraishi H, Ohta S, Suzuki S, Arima K, Aoki S, Toda S, *et al.*** Periostin

promotes chronic allergic inflammation in response to Th2 cytokines. *J. Clin. Invest.* 2012; **122**:2590–2600.

45. **Gillan L**, **Matei D**, **Fishman DA**, **Gerbin CS**, **Karlan BY**, **Chang DD**. Periostin secreted by epithelial ovarian carcinoma is a ligand for alpha(V)beta(3) and alpha(V)beta(5) integrins and promotes cell motility. *Cancer Res.* 2002; **62**:5358–5364.

46. **Hu D**, **Liu S**, **Shi L**, **Li C**, **Wu L**, **Fan Z**. Cleavage of survivin by granzyme M triggers degradation of the survivin-X-linked inhibitor of apoptosis protein (XIAP) complex to free caspase activity leading to cytolysis of target tumor cells. *J. Biol. Chem.* 2010; **285**:18326–18335.

47. **Anthony DA, Andrews D, Chow M, Watt S, House C, Akira S, Bird P, *et al.*** A Role for Granzyme M in TLR4-Driven Inflammation and Endotoxicosis. *J. Immunol.* 2010; **185**:1794–1803.

48. **van Domselaar R**, **Philippen LE**, **Quadir R**, **Wiertz EJ**, **Kummer JA**, **Bovenschen N**. Noncytotoxic inhibition of cytomegalovirus replication through NK cell protease granzyme M-mediated cleavage of viral phosphoprotein 71. *J. Immunol.* 2010; **185**:7605–13.

49. **Cullen SP**, **Afonina IS**, **Donadini R**, **Luethi AU**, **Medema JP**, **Bird PI**, **Martin SJ**. Nucleophosmin is cleaved and inactivated by the cytotoxic granule protease granzyme M during natural killer cell-mediated killing. *J. Biol. Chem.* 2009; **284**:5137–5147.

50. **Bovenschen N, de Koning P, Quadir R, Broekhuizen R, Damen J, Froelich CJ, Slijper M, *et al.*** NK Cell Protease Granzyme M Targets alpha-Tubulin and Disorganizes the Microtubule Network. *J. Immunol.* 2008; **180**:8184–8191.

51. **Lu H**, **Hou Q**, **Zhao T**, **Zhang H**, **Zhang Q**, **Wu L**, **Fan Z**. Granzyme M directly cleaves inhibitor of caspase-activated DNase (CAD) to unleash CAD leading to DNA fragmentation.

J. Immunol. 2006; **177**:1171–1178.

52. **Dutta B, Ren Y, Hao P, Sim KH, Cheow E, Adav S, Tam JP, *et al.*** Profiling of the Chromatin-Associated Proteome Identifies HP1BP3 as a Novel Regulator of Cell Cycle Progression. *Mol. Cell. Proteomics*. 2014:2183–2197.

53. **Chen FH**, **Thomas AO**, **Hecht JT**, **Goldring MB**, **Lawler J**. Cartilage oligomeric matrix protein/thrombospondin 5 supports chondrocyte attachment through interaction with integrins. *J. Biol. Chem.* 2005; **280**:32655–32661.

54. **Ewen CL**, **Kane KP**, **Bleackley RC**. A quarter century of granzymes. *Cell Death Differ.* 2012; **19**:28–35.

55. **Andrade F**, **Fellows E**, **Jenne DE**, **Rosen A**, **Young CSH**. Granzyme H destroys the function of critical adenoviral proteins required for viral DNA replication and granzyme B inhibition. *EMBO J.* 2007; **26**:2148–2157.

56. **Waterhouse NJ**, **Trapani J a.** H is for helper: granzyme H helps granzyme B kill adenovirus-infected cells. *Trends Immunol.* 2007; **28**:373–375.

57. **Ahel I**, **Ahel D**, **Matsusaka T**, **Clark AJ**, **Pines J**, **Boulton SJ**, **West SC**. Poly(ADP-ribose)-binding zinc finger motifs in DNA repair/checkpoint proteins. *Nature*. 2008; **451**:81–85.

58. **Maruyama T**, **Nara K**, **Yoshikawa H**, **Suzuki N**. Txk, a member of the non-receptor tyrosine kinase of the Tec family, forms a complex with poly(ADP-ribose) polymerase 1 and elongation factor 1α and regulates interferon-γ gene transcription in Th1 cells. *Clin. Exp. Immunol.* 2007; **147**:164–175.

59. **Snyder M**, **Huang XY**, **Zhang JJ**. The minichromosome maintenance proteins 2-7

(MCM2-7) are necessary for RNA polymerase II (Pol II)-mediated transcription. *J. Biol. Chem.* 2009; **284**:13466–13472.

60. **Karageorgos L**, **Guo X**, **Blanch L**, **Weber B**, **Anson D**, **Scot H**, **Hopwood J**. Structure and sequence of the human sulphamidase gene. *DNA Res.* 1996; **3**:269–71.

61. **Thomas DDH**, **Frey CL**, **Messenger SW**, **August BK**, **Groblewski GE**. A Role for Tumor Protein TPD52 Phosphorylation in Endomembrane Trafficking During Cytokinesis. *Biochem Biophys Res Commun*. 2010; **402**:583–587.

TABLES

Table 1 List of proteins differentially expressed by CD56^{neg} and CD56^{dim} NK cells in total proteome analysis. Proteins were identified by mass spectrometric analysis of isolated NK cell subsets. Proteins are listed here with their UniProt identification name and number, with corresponding Median Log_2 regulation factors of donor 4, 5, 6 and 7. The MAD is shown as indicator for donor specific deviations. The function of the protein is listed and corresponding references.

	Protein name	UniProt Name & Number	Median log^2-RF of H4-H7	MAD (H4-H7)	Function	References
	Up-regulated (CD56^{neg} > CD56^{dim})					
1	Myeloperoxidase	PERM P05164	1.69	0.64	Involved in protease processing, inflammation and bactericidal responses. Produces cytotoxic hypohalous acids (HOCL, HOBr, HOI) using H_2O_2.	Klebanoff et al. 2013 [37], Eiserich et al. 1999 [41]
2	High mobility group protein B2	HMGB2 P26583	1.31	0.89	DNA-bending protein involved in DNA repair. Chemoattractant for inflammatory cells.	Pusterla et al. 2009 [42], Zimmerman et al. 2008 [43]

3	Periostin	POSTN Q15063	1.41	0.84	Extracellular matrix protein supporting cell adhesion and migration. Modulates cell function via integrins and the PI3KAkt pathway.	Masuoka et al. 2012 [44], Gillan et al. 2002 [45]
4	Granzyme M	GRAM P51124	1.12	0.57	Cytotoxic molecule that induces caspase-dependent and -independent cell death in the target cell. Disrupts the microtubule network by cleaving the actin-plasma membrane linker ezrin and α-tubulin. Co-localizes with MIP-1α in cytotoxic vesicles. Enhances MIP-1α secretion from NK cells and macrophages. Cleaves HCMV proteins, inhibiting viral replication.	Hu et al. 2010 [46], Anthony et al. 2010 [47], van Domselaar et al. 2010 [48] , Cullen et al. 2009 [49], Bovenschen et al. 2008 [50], Lu et al. 2006 [51]
5	Heterochromatin protein 1-binding protein 3	HP1B3 Q5SSJ5	1.50	1.26	Influences cell proliferation by maintaining heterochromatin integrity during G1/S progression.	Dutta et al. 2014 [52]
6	Cartilage oligomeric matrix protein	COMP P49747	1.02	0.05	Interacts with multiple ECM components. Enhances cellular attachment.	Chen et al. 2005 [53]
7	Granzyme H	GRAH P20718	0.96	0.32	Cytotoxic molecule. Induces caspase-dependent and -independent target cell death. Cleaves adenovirus protein, inhibiting viral replication.	Ewen et al. 2012 [54], Andrade et al. 2007 [55], Waterhouse et al. 2007 [56]
8	Poly [ADP-ribose] polymerase 1	PARP1 P09874	1.20	1.13	Involved in DNA repair. In complex with Txk and EF-1α activates IFN-γ promoter transcription in Th1 cells.	Ahel et al. 2008 [57], Maruyama et al. 2007 [58]
9	DNA replication licensing factor MCM5	MCM5 P33992	1.14	0.53	Replicative helicase component essential for DNA replication. Also involved in transcription.	Snyder et al. 2009 [59]
	Down-regulated ($CD56^{neg}$ < $CD56^{dim}$)					
1	N-sulpho-glucosamine sulphohydrolase	SPHM P51688	-1.09	0.47	Lysosomal hydrolase (sulfatase) involved in the processing of glycosaminoglycan heparan sulphate.	Karageorgos et al. 1996 [60]
2	Tumor protein D52	TPD52 P55327	-0.96	0.11	Regulates lysosome trafficking. Induces LAMP-1 accumulation at the plasma membrane.	Thomas et al., 2009 [36] and 2010 [61]
3	Myosin regulatory light chain 12A	ML12A P19105	-0.94	0.62	Maintains the stability of Myosin IIa. Actin-binding protein that enables interaction between lytic granules and F-actin. Mediates lytic granule transport through the F-actin mesh to the synaptic membrane and promotes their exocytosis.	Park et al. 2011 [32], Andzelm et al. 2007 [33], Watanabe et al. 2007 [34], Sanborn et al. 2009 [35]

Table 2 Relative abundance levels of granzymes in $CD56^{neg}$ compared to $CD56^{dim}$ NK cells. Granzyme (Grz) abundances are calculated and depicted as $\log_2$ regulation factors for four donors (H4-H7). Low MAD values indicate low donor variation of granzyme

abundances. GrzH and GrzM (grey) showed superior levels combined with low donor variation in $CD56^{neg}$ compared to $CD56^{dim}$ NK cells in at least three out of the four donors.

	$CD56^{neg/dim}$						
	H4	**H5**	**H6**	**H7**	**MAD**	**mean**	**median**
GrzA	1.53	2.49	0.73	0.28	1.26	1.257	1.13
GrzB	NA	1.83	0.36	0.46	0.22	0.880	0.46
GrzH	0.96	1.69	0.95	0.65	0.32	1.063	0.955
GrzK	NA	1.88	0.28	0.22	0.12	0.793	0.28
GrzM	1.08	1.65	0.50	1.15	0.57	1.095	1.12

FIGURE LEGENDS

Figure 1: $CD56^{neg}$ NK cells phenotyping. NK cell subsets were analysed by flow cytometry as part of PBMCs isolated from the blood of healthy individuals. Information on mAbs and the gating strategies for NK cell subset identification are provided in the materials & methods. (A) Mean fluorescence intensities (MFI) of CD56, NKp46, EOMES and T-bet of primary human $CD56^{bright}$ (blue), $CD56^{dim}$ (red) and $CD56^{neg}$ (green) NK cells were analysed in four donors (n=4). Symbols represent the mean of two replicates for each donor. Two experiments with two donors per experiment were performed. Additionally, the MFI from all four donors was calculated (black bar). Two-tailed paired t-test with Bonferroni-Holm correction was performed (* $p<0.05$). (B, C) Dendrogram received from the Ward's clustering analysis of the mean surface marker expression intensity obtained by flow cytometry of the three NK cell subsets, T cells, and the rest of the lymphocytes (dump) from PBMCs of human donors H1-H3 (n=3). Data are pooled from 3 experiments with 1 donor per experiment. Triangles highlight NK cell subset specific markers. (D) Principal component analysis (PCA) plot of 57 surface markers segregating the three NK cell subsets. The calculation is based on the mean surface marker expression from donors H1-H3. Symbols

correspond to clusters highlighted in Supporting Information Figure 2. The correlation matrix values between the NK cell subsets are $C_{CD56dim/bright}$=0.6411; $C_{CD56neg/bright}$=0.7207 and $C_{CD56neg/dim}$=0.9207.

Figure 1

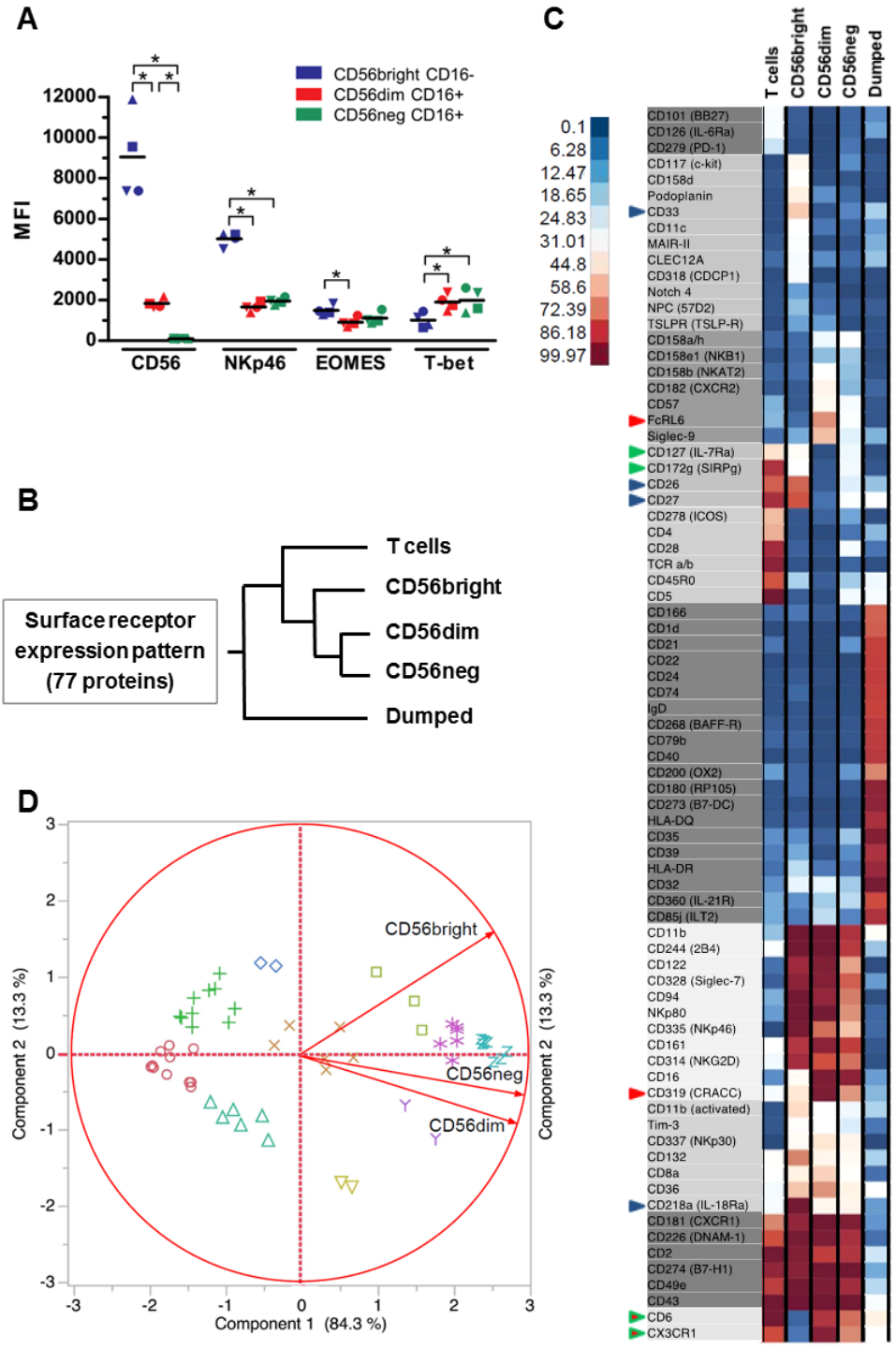

Figure 2: Total proteome analysis of CD56$^{neg/dim/bright}$ NK cells. (A) Experimental design of MS-based total proteome analysis. CD56^{bright} CD16^{-}, CD56^{dim} CD16^{+} and CD56^{neg} CD16^{+} NK cells, all CD3/CD14/CD19^{-} CD7^{+}, were sorted from PBMCs of four healthy individual donors (logarithmic scaling in CD56/CD16 plot). Proteins were then precipitated and tryptic peptides were subset-specifically labelled (iTRAQ^{TM} technology), combined, fractionated with strong cation-exchange chromatography (SCX) and quantitatively sequenced by LC-MS/MS. NK cell subset-specific comparison of MS signals and calculation of relative protein abundances are based on subset-specific isobaric labelling. (B) Subset-specific pathway analysis including 10% of the (up-) regulated proteomic data (in 3 of 4 donors making 1669 proteins) using DAVID and the implemented KEGG pathways. The bar chart shows the number of identified proteins covering NK cell specific pathways in a subset-specific manner (EASE score: $p^{*}<0.05$; calculated by a modified Fisher exact test). (C) Number of donor-independently and subset-specifically regulated proteins identified by statistical MS data evaluation of four independent proteome experiments (H4-H7). Up-regulated proteins are displayed in red and down-regulated in blue. Protein name, regulatory information and protein functions are summarized in Supporting Information Table 4.

Figure 2

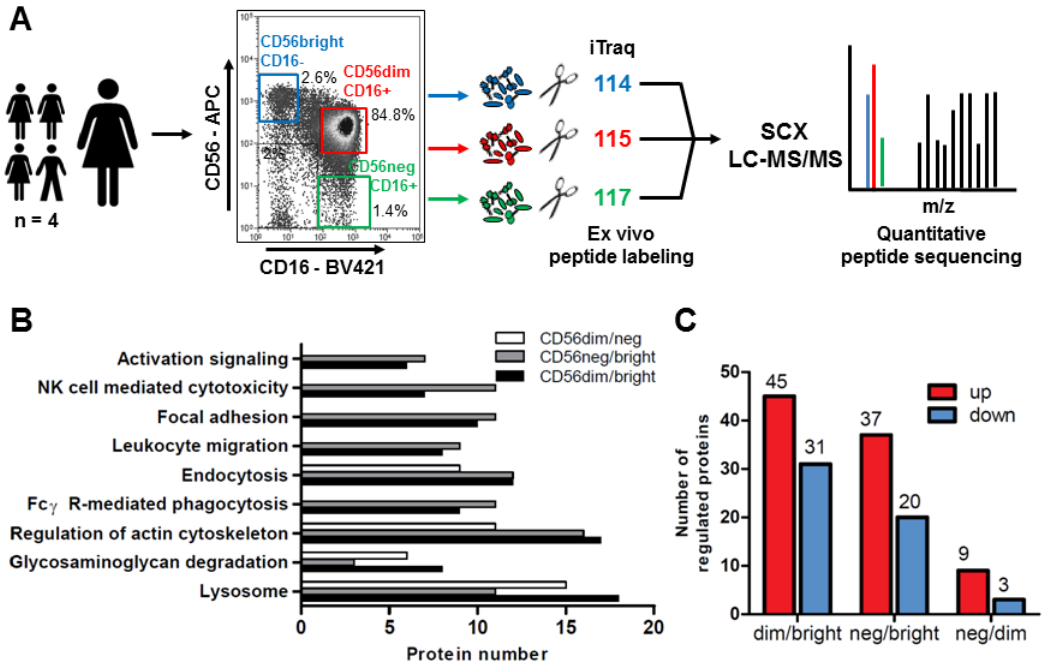

Figure 3: Functional inventory model of CD56^{neg} NK cells in comparison to CD56^{dim} and CD56^{bright} NK cells. Differentially abundant proteins of the three NK cell subsets of healthy humans were determined in the surface (n=3; shown in Fig. 1C) and the total proteome analysis (n=4; shown in Fig. 2C). Selected proteins are sorted according to their function: “Activation and inhibition“ (blue), “Adhesion“ (green), “Immune synapse formation and cytotoxicity“ (orange), “Lytic granule“ (red) and “Other” (black). Protein expression intensities of receptors detected in the surface screen are visualized with * for low, ** for intermediate and *** for high expression. ° marks surface proteins exclusively detected by MS. Shapes of the surface receptors indicate in which NK cell subsets the receptor plays a role. Sketched are the microtubules along which the lytic granules move toward the microtubule organizing center, the filamentous actin network (black bars) at the immune synapse and the release of the lytic granules (red dots) into the NK-target cell synapse. The displayed number of granules correlates with the observed cytotoxic capacity to lyse K562 target cells, as shown in Fig. 4C.

Figure 3

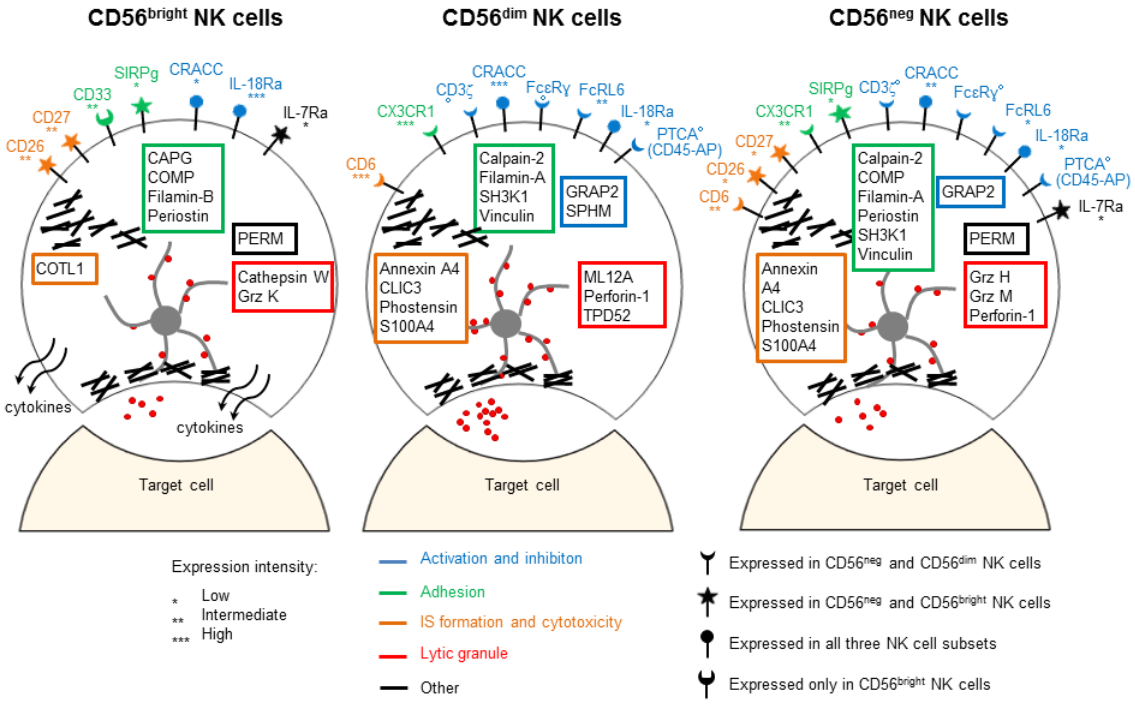

Figure 4: Moderate in vitro responsiveness of natural CD56^{neg} NK cells. (A) Degranulation was measured as CD107a surface accumulation after stimulation *via* IL-12/15/18 alone, or *via* K562 (E:T 2:1) alone, or *via* interleukin cocktail plus K562 (E:T 2:1) in a subset-specific way (n=4 donors). (B) Same stimulation conditions were used to induce IFN-γ release, which was measured after intracellular staining using flow cytometry (n=3 donors). Exception for controls due to pre-activation caused by the sorting process: data for only two donors (A, B) is shown. (C) Cytotoxicity of sorted primary human NK cell subsets was assessed by measuring CFSE^{pos}7AAD^{pos} K562 target cells after E:T specific co-culture using flow cytometry (n=3 donors). Different colours code the NK cell subsets, shapes represent individual donors. Donors in (A) and (B) with corresponding shapes are identical. Each data set is pooled from two experiments and based on sorted NK cell subsets. Two biological replicates per condition and NK cell subset were analysed. Exception in (C) due to limited cellular material: one replicate in two donors for CD56^{neg} and one replicate in one donor for CD56^{bright} NK cells. For co-culture at 16:1 only one donor for CD56^{neg} NK cells delivered sufficient cellular material. Statistics was performed using GraphPad. In (A, B) two-way ANOVA with Bonferroni-Holm correction was performed to analyse NK cell subset-specific differences (black bars, black asterisk) and to compare effectiveness of stimulation condition on activation (grey bar, coloured asterisks corresponding to the NK cell subsets. In (C) the two-tailed paired t-test with Bonferroni-Holm correction was applied (* $p<0.05$). Individual values for all donors and their mean are shown. In (C) the line connects the mean of the three donors.

Figure 4